ORIGINAL CONTRIBUTION

CrossMark

Measuring and assessing first and second normal stress differences of polymeric fluids with a modular cone-partitioned plate geometry

Salvatore Costanzo [1,2,3] · Giovanni Ianniruberto [4] · Giuseppe Marrucci [4] · Dimitris Vlassopoulos [1,2]

Abstract
We propose a simple, robust method to measure both the first and second normal stress differences of polymers, hence obtaining the full set of viscometric material functions in nonlinear shear flow. The method is based on the use of a modular cone-partitioned plate (CPP) setup with two different diameters of the inner plate, mounted on a rotational strain-controlled rheometer. The use of CPP allows extending the measured range of shear rates without edge fracture problems. The main advantage of such a protocol is that it overcomes limitations of previous approaches based on CPP (moderate temperatures not exceeding 120 °C, multiple measurements of samples with different volume) and yields data over a wide temperature range by performing a two-step measurement on two different samples with the same volume. The method was tested with two entangled polystyrene solutions at elevated temperatures, and the results were favorably compared with both the limited literature data on the second normal stress difference and the predictions obtained with a recent tube-based model of entangled polymers accounting for shear flow-induced molecular tumbling. Limitations and possible improvements of the proposed simple experimental protocol are also discussed.

Keywords Start-up experiment · Second normal stress difference · Cone-partitioned plate rheometry

Introduction

One of the most intriguing features of viscoelastic fluids, and in particular of polymers, undergoing nonlinear shear is their ability to develop two nonzero normal stress differences (Bird et al. 1977; Macosko 1994). Normal stresses are responsible, among other things, for a variety of flow instabilities which are relevant for polymer processing, such as extrudate swell (Boger and Walters 1993), sharkskin (Miller and Rothstein 2004), and edge fracture (Tanner and Keentok 1983). In particular, the second normal stress difference is associated with edge fracture

instabilities in rotational shear flows (Tanner and Keentok 1983; Skorski and Olmsted 2011; Hemingway et al. 2017). A complete characterization of the flow behavior of a specific polymeric system should provide the dependence of the three viscometric functions, i.e., viscosity (η), first and second normal stress differences (N_1 and N_2), upon shear rate ($\dot{\gamma}$). As the appearance of normal stresses in viscoelastic materials undergoing shear is a second-order effect, normal stress differences are usually presented in terms of normal stress coefficients, $\Psi_1 = N_1/\dot{\gamma}^2$ and $\Psi_2 = N_2/\dot{\gamma}^2$. Such functions are typically determined from transient start-up experiments in rotational shear rheometers (Gao et al. 1981; Meissner et al. 1989; Schweizer 2002; Baek and Magda 2003; Schweizer et al. 2008). However, obtaining reliable data in fast rotational flows is not trivial because of the possible development of instabilities such as wall slip, shear banding, and edge fracture. The latter is inevitable and yields voids in the measured specimen, hence leading to underestimation of viscosity and normal stresses. Moreover, It can also result in a departure from the linear velocity profile in the rheometer fixture, akin to shear banding signature (Schweizer and Stöckli 2008). The larger the fracture, the larger is the error in evaluating η, N_1, and N_2. A good strategy to overcome this problem is to use a cone-partitioned

✉ Salvatore Costanzo
salvatore.costanzo@umontpellier.fr

1 Institute of Electronic Structure and Laser, Foundation for Research and Technology (FORTH), 71110 Heraklion, Crete, Greece

2 Department of Materials Science and Technology, University of Crete, 71110 Heraklion, Crete, Greece

3 Present address: Laboratoire Charles Coulomb UMR 5221, Université Montpellier 2, 34095 Montpellier, France

4 Department of Chemical, Materials, and Production Engineering, Federico II University, 80125 Naples, Italy

plate (CPP) geometry (Meissner et al. 1989; Snijkers and Vlassopoulos 2011; Schweizer and Schmidheiny 2013; Costanzo et al. 2016). Such geometry restricts the measurement volume to the inner part of the sample so that edge distortions do not affect the measurements. However, a CPP geometry with a single partition can provide reliable measurements only for viscosity. In modern rotational rheometers, N_1 can be directly accessed by means of axial transducers. However, the value of N_1 recorded in rheometers equipped with a CPP geometry is an apparent one (N_{app}) because of the contribution to the normal stress distribution coming from the part of the sample exceeding the transducer area. Such contribution causes a nonnegligible overestimation of N_1 (Schweizer and Bardow 2006; Costanzo et al. 2016). Furthermore, N_2 cannot be obtained from direct viscometric measurements (Macosko 1994; Tanner 2000). A brief historical survey follows.

Early on (Kotaka et al. 1959; Lodge 1964; Bird et al. 1977), it was realized that rotational rheometry can be used for measuring the normal stress distribution in cone-plate (CP) or parallel-plate (PP) geometries, starting from the equations of fluid motion. In particular, it was shown that a combination of CP (which provides N_1) and PP (which provides N_1-N_2) geometries gives access to both normal stress differences (Kotaka et al. 1959; Adams and Lodge 1964; Ginn and Metzner 1969; Savins and Metzner 1970; Barnes et al. 1975; Eggers and Schümmer 1994). Even the use of cone and plate only with varying the truncation gap was shown to be an efficient method to probe N_2 (Kotaka et al. 1959; Lodge 1964; Jackson and Kaye 1966; Marsh and Pearson 1968; Kulicke and Wallbaum 1985; Ohl and Gleissle 1992). These methods have been recently used and/or modified in order to measure the normal stresses in shear thickening (Cwalina and Wagner 2014) and non-Brownian (Sing and Nott 2003; Gamonpilas et al. 2016) colloidal suspensions. However, problems such as edge fracture make the implementation of this straightforward approach very difficult, if not impossible, especially for highly viscoelastic fluids (e.g., polymer melts) and for a reasonable range of shear rates (Tanner 1970). In general, viscometric flows with polymer melts are far more challenging than with polymer solutions; hence, most of the relevant experimental work to obtain N_2 concerns the latter (Harris 1968; Ginn and Metzner 1969; Pritchard 1971; Tanner 1973), and it is limited to low shear rates. Different methods to obtain N_2 based on visual observation were proposed, with reasonable success: for example, measuring the shape of the free surface of polymeric fluids flowing down a semicircular channel (Wineman and Pipkin 1966; Kuo and Tanner 1972; Kuo and Tanner 1974; Keentok et al. 1980; Sturges and Joseph 1980) or analyzing the edge effects in a cone-and-plate fixture (Tanner 1970). The open channel flow approach has been used to measure N_2 in non-Brownian suspensions as well (Couturier et al. 2011). Rheo-optical methods have been proven to be a

particularly useful tool for determining normal stresses and, in fact, the full stress tensor in viscoelastic solutions, by means of the stress optical law (Brown et al. 1995; Takahashi and Fuller 1996; Kalogrianitis and van Egmond 1997; Takahashi et al. 2002). However, besides again being restricted to solutions (and usually at room temperatures), these approaches are very sensitive to fine alignment issues, especially the oblique angle case (Takahashi and Fuller 1996; Takahashi et al. 2002), rendering their use quite limited.

Focusing on rotational rheometry and highly viscoelastic polymeric fluids, the most effective methods to measure the normal stress differences are based on the evaluation of the normal stress distribution in CP geometry (Kotaka et al. 1959; Lodge 1964) with constant shear rate ($\dot{\gamma}$) along the radial direction. The use of flush-mounted transducers on the plate at different radii of the sample, taking advantage of the hole pressure analysis, yielded high-quality data (Tanner and Pipkin 1969; Higashitani and Pritchard 1972; Kearsley 1973; Christiansen and Leppard 1974; Baird 1975; Boger and Denn 1980; Gao et al. 1981; Magda et al. 1991; Lodge 1993; Lee et al. 2002; Baek and Magda 2003; Alcoutlabi et al. 2009). However, this approach is limited to low temperatures because the pressure sensors cannot withstand the very high temperatures which are relevant for polymer melt flow. In addition, inserting a transducer at different radii requires a large sample radius and therefore large sample quantities. An alternative approach is to measure the normal force acting on partitions of the plate with different radii by means of a CPP geometry (Schweizer 2002; Schweizer et al. 2004). While this method works also at relatively high temperatures, it requires multiple measurements (see the next section for details), generally from 4 to 6 per shear rate (Schweizer 2002; Schweizer et al. 2004), with samples of different radii. Therefore, it requires the preparation of samples with different masses, and several loadings, rendering the measurements tedious and time-consuming, while introducing more sources of error. This can be overcome by means of a CPP geometry with two partitions, the so-called "CPP-3" (Schweizer and Schmidheiny 2013), which represents the state of the art in CPP design. While it will be discussed in more detail in the next section, we note that its small temperature range (from room temperature to about 120 °C) and its sophisticated implementation limit its use. Hence, there is a need to optimally combine accuracy, high temperatures, small amounts of sample, and easiness of use.

In this work, we attempt at addressing this challenge and propose a simple CPP-based method to obtain steady-state values of N_1 and N_2 in a two-step measurement with two identical samples over a wide temperature and shear rate range. The paper is organized as follows: after this introduction, we briefly present the historical development of the CPP geometry and its implementation for measuring N_1 and N_2. Then, our modular homemade CPP setup for the ARES

rheometer is described. Next, the protocol for obtaining N_1 and N_2 is applied to two polystyrene solutions in an oligostyrene solvent at high temperatures. The experimental results are compared with predictions of a recent tube-based model accounting for flow-induced molecular tumbling (Costanzo et al. 2016). In particular, the model assumes that shear start-up tumbling reduces the chain stretch typical of fast flows, suppressing it completely at steady state. The latter feature has been recently examined by Khomami and co-workers (Nafar Sefiddashti et al. 2015), who concluded that tumbling appears to affect the orientational contribution to the steady-state stress rather than that due to chain stretch. Their analysis, however, assumes a single Maxwell-like relaxation time, while our model applies to a multimode relaxation spectrum. Finally, the main conclusions are summarized in the last section.

Historical background of CPP geometry

Evidence of edge fracture instability in shear flows was first reported in the early works of Pollett and Cross (1950), Pollett (1955), Tanner and Keentok (1983), and Keentok and Xue (1999). In particular, Tanner and Keentok (1983) established a correlation between the magnitude of N_2, the surface tension, and the amplitude of the fracture. They found that edge fracture occurs when

$$|N_2| > 2\Gamma/(3h) \tag{1}$$

where Γ is the surface tension and h is the size of the fracture. This expression was derived by assuming an initial semicircular crack and a second-order fluid. Therefore, its application is not general. Very recently, a theoretical study of the edge fracture instability was performed by Fielding and co-workers (Hemingway et al. 2017) for more general constitutive models (Johnson-Segalman and Giesekus). They derived an exact analytical expression for the onset of the instability in shear flows. In particular, they found that the jump in shear stress across the interface between the fluid and the outside medium is a relevant parameter to determine the fracture. The generalized criterion for fracture is

$$\frac{1}{2}\Delta\sigma \frac{d|N_2(\dot{\gamma})|}{d\dot{\gamma}} \bigg/ \frac{d\sigma}{d\dot{\gamma}} > \frac{2\pi\Gamma}{L_y} \tag{2}$$

where σ is the shear stress, $\Delta\sigma$ the jump in shear stress across the interface between fluid and surrounding medium (which is equal to σ when the medium is air with negligible viscosity), and L_y the gap size. These authors used a cylindrical Couette geometry in their calculations; hence, the respective L_y for CP should be the outer gap. In the limit of small shear rates, where $N_2 \sim \dot{\gamma}^2$ and $\sigma = \eta\dot{\gamma}$ (η being the viscosity), and for $L_y = h$, the above expression of Tanner is recovered. We note for

completeness that often shear banding instabilities are triggered by edge fracture. Their link has been addressed experimentally (Schweizer and Stöckli 2008) and theoretically (Skorski and Olmsted 2011).

The first experimental attempt to overcome the edge fracture issue in rotational rheometers was reported by Meissner and co-workers in 1989 (Meissner et al. 1989). They modified a commercial RMS800 rotational rheometer and equipped it with a CPP fixture to measure the viscometric functions of LDPE samples. In order to extract N_2, they used a fixed inner radius of 6 mm and varied the outer radius. Temperature control of this setup was provided by electrically heated tools to ensure a good temperature homogeneity of the sample. The experimental procedure adopted by Meissner and co-workers to measure N_2 is based on the following equation, (Bird et al. 1977; Schweizer 2002)

$$N_{app} = \frac{2F}{\pi R_{stem}^2} = N_1 + 2(N_1 + 2N_2)\ln\left(\frac{R}{R_{stem}}\right) \tag{3}$$

where N_{app} is the normal force per unit area detected by the axial transducer on the inner partition (apparent value of N_1), F the normal force acting on the inner plate, R_{stem} the radius of the inner plate, and R the radius of the sample. This procedure involves multiple measurements for each shear rate. The normal stress differences are thereby evaluated from the slope and the intercept of the linear function N_{app} vs. $\ln(R / R_{stem})$. The radius (R) is estimated from the mass (m) of the sample, according to the equation

$$R = \sqrt[3]{\frac{3m}{2\pi\rho\theta}} \tag{4}$$

where ρ is the sample density and θ the cone angle (Meissner et al. 1989; Schweizer 2002). The same method was used by Schweizer (2002) in order to measure the viscometric functions of a polystyrene melt with $M_w = 158$ kg/mol at 190 °C. Schweizer et al. (2004) also measured a polystyrene melt with $M_w = 200$ kg/mol at 175 °C. In the latter case, the inner radius was reduced to 4 mm in order to avoid early overload of the axial transducer of the instrument. In this regard, problems associated with the axial compliance of the instrument were addressed by several authors (Hansen and Nazem 1975; Macosko 1994; Kasehagen and Macosko 1998; Schweizer and Bardow 2006; Crawley and Graessley 2015; Meissner 1972). It was found that the axial compliance induces delays in the axial force signal of rotational rheometers. Since axial compliance cannot be completely eliminated, delays affecting N_1 or N_{app} signals are unavoidable in transient shear start-up measurements; therefore, reliable data are restricted to the steady-state values of the normal force (Schweizer and Bardow 2006; Costanzo et al. 2016). In order to reduce the

axial compliance and increase the normal force maximum load, a homemade rheometer (MTR 25) with normal force capacity of 25 kg and large axial stiffness of 10^7 N/m was developed (Schweizer et al. 2008). The MTR 25 had another important characteristic: by means of two axial transducers, the normal force of both the inner and the outer partitions could be probed. This enabled the simultaneous determination of N_1 and N_2 in a single start-up experiment. In fact, this strategy was first implemented by Pollett (1955); however, its main drawback is that the measurement on the part of the sample in the outer partition is affected by edge fracture. Moreover, the use of MTR 25 requires large quantities of sample, as the outer radius is around 10–15 mm.

The above problem was addressed with the design of the CPP-3 cell (Schweizer and Schmidheiny 2013). This geometry, consisting of three partitions, accommodates very small amounts of sample (order of tens of milligrams) and has been implemented on a MCR 502 rheometer (Anton Paar, Germany). It consists of an inner measuring partition with radius R_1, a middle measuring ring with external radius R_2, and an outer nonmeasuring partition to prevent edge fracture. The latter is fixed on the rheometer frame and contains the outer part of the fluid, which will experience fracture at high shear rates. The working principle is similar to that of the MTR 25. Here, the outer radius is fixed, and the distribution of normal stresses is integrated over two different radii. The N_1 and N_2 signals are therefore obtained by iterating Eq. (3) for the two partitions with a fixed outer radius R

$$N_{app,1} = \frac{2F_1}{\pi R_1^2} = N_1 + 2(N_1 + 2N_2)\ln\left(\frac{R}{R_1}\right) \tag{5}$$

$$N_{app,2} = \frac{2(F_1 + F_2)}{\pi R_2^2} = N_1 + 2(N_1 + 2N_2)\ln\left(\frac{R}{R_2}\right) \tag{6}$$

In Eqs. (5)–(6), the geometrical parameters are known, as well as $N_{app,1}$ and $N_{app,2}$, which are the apparent normal forces (per unit area) detected on partition 1 and both partitions 1 and 2, respectively. The only two unknowns are N_1 and N_2, which can therefore be determined. Besides the difficulty of use (in the current design, the rheometer is used to shear the material,

and the two normal forces are measured independently with external transducers; hence, alignment and temperature equilibration of the partitions are very involved procedures), a disadvantage of this technique is the upper temperature limit (Schweizer and Schmidheiny 2013) of about 120 °C, which is rather restrictive for many polymer melts.

Recently, a CPP setup was developed for the ARES rheometer (Snijkers and Vlassopoulos 2011). Such a fixture is similar to that of Meissner et al. (1989), but an extension of the convection oven of the ARES rheometer was needed in order to achieve good temperature control at high temperatures, and several checks were necessary to ensure the absence of nonnegligible temperature gradients. This tool is useful only for obtaining reliable viscosity measurements at high temperatures, but it is not helpful for N_2. A similar setup was also used on the ARES rheometer by Ravindranath and Wang (2008). The temperature problem was overcome with a new design of CPP for the ARES (Costanzo et al. 2016). In the next section, we present the modular CPP based on this design and its use for measuring N_1 and N_2.

Homemade CPP setup to detect N_1 and N_2

Figure 1a shows a schematic of our homemade CPP setup while Fig. 1b shows a photograph of the actual fixture. The bottom cone is attached to the motor of the ARES rheometer. An appropriately modified version can be implemented on the MCR 702 (a twin-drive rheometer with two motors, from Anton Paar, Austria) as well, with the motor separated (say at the bottom) from the transducer (at the top). For measuring polymer melts and solutions, we used a standard cone with a diameter of 25 mm and a cone angle (θ) of 0.1 rad. Such a value of θ represents a good compromise between the necessity to reduce axial compliance (Macosko 1994; Schweizer and Bardow 2006; Crawley and Graessley 2015) and the need of preventing edge fracture and potential shear banding instabilities (Lee et al. 2002; Sui and McKenna 2007; Schweizer and Schmidheiny 2013). Indeed, normal forces originating in fast shear start-up tend to push the tools apart, resulting in a

Fig. 1 **a** Schematic of the CPP with a single partition. **b** Photo of the CPP for ARES rheometers
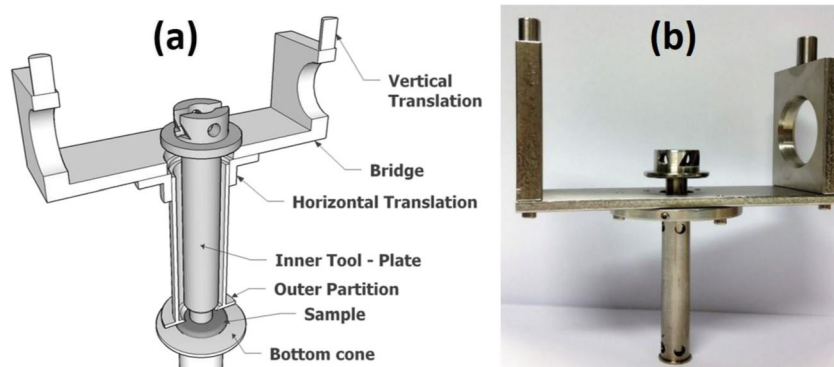
squeeze flow which occurs over a characteristic time scale: $t_a = (6\pi R\eta) / (K_a\theta^3)$, where R is the radius of the sample and K_a the axial stiffness (Schweizer and Bardow 2006). The squeeze flow delays the normal force signal by a time which scales linearly with t_a.

Therefore, the larger the θ, the smaller is the t_a and the smaller the delay of the normal force signal. On the other hand, a larger cone angle implies a larger gap at the edge of the sample. Such a condition enhances edge fracture (Sui and McKenna 2007; Schweizer and Stöckli 2008; Skorski and Olmsted 2011; Schweizer and Schmidheiny 2013).

Concerning our setup, the inner partition is a homemade stainless steel plate with a diameter of 6 mm. The inner shaft has a slender body compared to the standard tools of ARES rheometers. The reason for this choice is to provide enough space around the shaft to house the outer partition so that the geometry can fit into the ARES convection oven. The outer partition is a nonmeasuring ring with an inner diameter of 6.2 mm and an outer diameter of 15 mm. Hence, the gap between the inner shaft and the outer partition is 0.1 mm. Such a small value is necessary in order to delay the penetration of the test material into the gap. The outer partition is attached to a hollow bridge by means of a horizontal translation stage (which is, in fact, a plate with screws, allowing manual translation and coarse position adjustment). The outer partition and the translation stage are fixed together by means of three screws. The translation stage is attached to the hollow bridge through three tap bolts. The holes into the translation stage are 0.5 mm larger than the diameter of the tap bolts. Such a mechanical tolerance serves to align the outer partition concentrically to the shaft. The tap bolts can be loosened so that the translation stage is free to translate on the plane parallel to the shaft direction. The horizontal alignment is checked by eye with the help of a mirror placed on the lower plate at an angle of 45° with respect to the plate itself. After the outer partition is aligned concentrically with the shaft, the tap bolts are tightened to block the translation. To help with the alignment process, the translation of the outer partition is guided by means of an outer corona with three screws that press around the stage (not shown in Fig. 1 for clarity of the drawing). The hollow bridge possesses two cylindrical attachments at the edge for vertical alignment. They slide into the holes of the rheometer head and are fixed by means of passing-through screws.

In order to achieve a good alignment, we perform the following operations: (i) the inner shaft is mounted at the top while a plate fixture (with a diameter of 25 or 50 mm) is attached at the bottom; (ii) the gap is zeroed; (iii) the upper stage is raised to the top position, and the bridge with the outer partition is inserted into the head of the rheometer; (iv) the upper stage is brought back to the zero position, and the hollow bridge is allowed to slide down until it sits on the bottom plate together with the inner shaft; this operation ensures vertical alignment and parallelism of the inner tool and of the outer partition; (v)

after vertical alignment is achieved, the bridge is locked into the head of the rheometer by means of two screws; (vi) the head of the rheometer is raised from the lower plate, and a mirror is placed on the lower plate to check for horizontal alignment; (vii) the translation stage on the hollow bridge is loosened and translated in order to achieve concentricity of the inner shaft and of the outer partition; (viii) the horizontal translation stage is blocked, and vertical alignment is re-checked by verifying the zero position of the whole geometry. If the new zero position varies by not more than 5 μm from the previous one, the alignment procedure is accepted, otherwise the whole operation is repeated. Once the alignment is satisfactory, we replace the bottom plate by the cone, and we zero the gap again. At this stage, the geometry is ready for sample loading. The test sample should be positioned symmetrically on the cone. Samples with a diameter of 8 mm are generally prepared for an inner partition with a diameter of 6 mm (called thereafter CPP-6). Hence, there is a challenge of properly centering a discotic specimen with a diameter of 8 mm on a cone with a diameter of 25 mm. This is done with the help of centering tools. Centering tools can be built in different ways. An easy approach consists in building a semicircular cap with an inner diameter of 25 mm, which fits the bottom cone. A semicircular 8-mm hole is carved in the middle of the semicircular cap. During the sample loading, the cap is placed on the cone and the sample is pressed against the 8-mm hole. Once the tool is removed, the sample remains well centered.

Our homemade CPP setup was appropriately modified in order to take advantage of the direct measurement of normal stresses at different radii while keeping good temperature control. With bulky geometries, thermal equilibration is generally an issue. In this regard, the main problem of the CPP is that the outer partition shields the inner shaft from the convection fluid circulating inside the oven. The thicker the walls of the outer partition, the larger is the thermal gradient between the inner and the outer tools. Concerning our setup, we tried to minimize the latter issue by making the walls of the outer partition as thin as possible, compatibly with the mechanical strength of the geometry. Both the hollow cylinder and the bottom corona of the outer tool are 1 mm thick. Furthermore, holes have been drilled at the top and the bottom of the outer cylinder, and at the bottom of the inner tool, in order to promote thermal convection between the inner and the outer tools. If the sample is allowed to equilibrate for at least 20–25 min before running the test, this configuration suffices to obtain a good thermal homogeneity of the sample. Figure 2 reports the comparison between a frequency sweep test performed on molten linear polystyrene ($M_w = 133k$, $T = 150$ °C) with only the inner tool (PP-6) and one performed with the complete CPP-6. The good agreement between the two experiments confirms that the thermal gradients induced by the use of the CPP are minimal.

Another issue that can arise in transient rotational rheometry concerns wall slip (Wang et al. 2011; Carotenuto
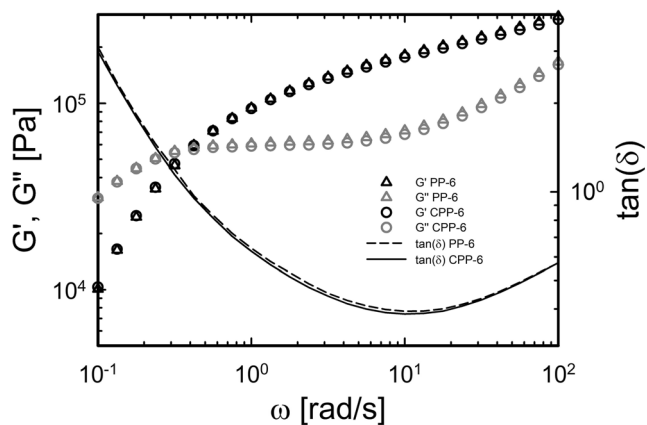
Fig. 2 Comparison between a frequency sweep experiment on molten linear polystyrene ($M_w = 133$k, $T = 150$ °C) performed with 6-mm parallel plates (PP-6) and the one performed with the CPP-6

et al. 2015). We did not observe any wall slip for the samples investigated here. However, if the tested systems are subject to wall slip, one can easily adopt roughened versions of both the inner tool and the outer corona in order to avoid such an issue. Due to the narrow gap between the partitions, the application of sandpaper to the CPP results to be very difficult.

Indeed, our design is modular, allowing for the inner shaft and the outer partition to be easily replaced. Therefore, we constructed another inner shaft that has a diameter of 10 mm and a corresponding outer partition with an inner diameter of 10.15 mm (CPP-10). The outer partitions of CPP-6 and CPP-10 setups have the same outer diameter and can be attached to the hollow bridge by means of the same translation stage. This is schematically depicted in Fig. 3.

The setup with two partitions mimics the functioning principle of Schweizer's CPP-3 setup and is based on the same

working equations (Eqs. (5)–(6)). However, in order to get the two signals of $N_{app,1}$ and $N_{app,2}$, we need to run two measurements with identical samples, instead of one. The advantage is that the temperature control and stability are ensured with the convection oven of the ARES rheometer; hence, measurements are reliable even at very high temperatures. It is also relatively easy to align and operate this CPP fixture, whereas the window of the oven provides partial optical control of the sheared sample. Disadvantages include the relatively low maximum normal force capacity of the axial transducer (maximum of 2 kg) and the noise of the signal of the normal force, which are associated with the specific ARES rheometer. This restricts detection of N_1 and N_2 to a relatively narrow range of shear rates. The lower limit is set by shear rate values high enough to obtain unambiguous signals of normal force. The upper limit is set by shear rates at which the normal force reaches the limit of 2 kg. In general, polymeric systems with reasonably low values of the plateau modulus (G_N^0; typically well below 1 MPa) are amenable to higher shear rates before overloading the transducer. Therefore, we diluted high-molar-mass polystyrene (PS) in oligostyrene in order to obtain two entangled solutions with appropriately low values of G_N^0.

Polystyrene solutions

Two solutions were prepared by diluting high-molar-mass PS in a 2k oligostyrene ($M_w = 2$ kg/mol). One solution was prepared by diluting PS with $M_w = 200$ kg/mol in the oligostyrene at $\phi = 0.5$ w/w. This solution is coded as PS200k-2k-50, where 50 refers to the weight percentage. The other solution was prepared by diluting PS with $M_w = 545$ kg/mol in the oligostyrene. The weight
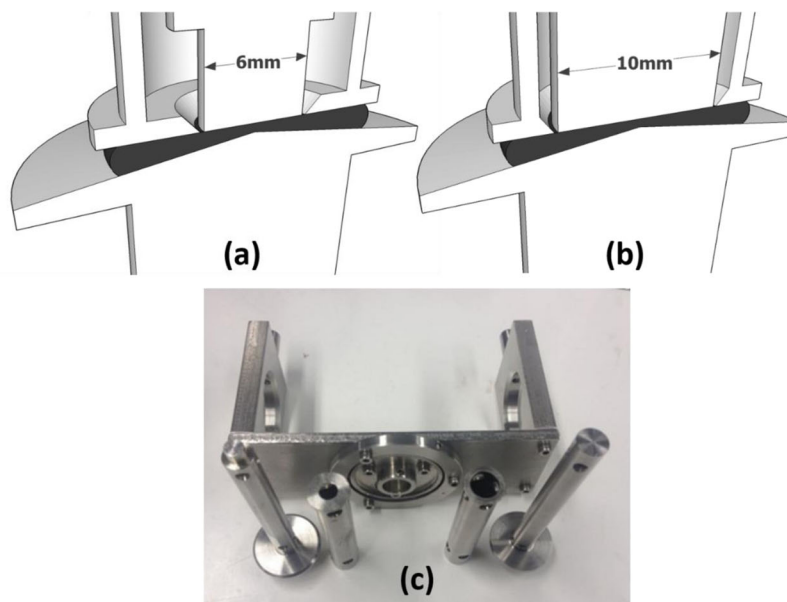

Fig. 3 Two different partitions to measure normal stresses with cone-partitioned plate. **a** 6-mm partition (CPP-6). **b** 10-mm partition (CPP-10). **c** Photograph of the actual setup with the two exchangeable partitions

percentage of PS was $\phi = 0.7$ *w/w*, and therefore the solution is coded as PS545k-2k-70. For the preparation of the solutions, the polymer was first dissolved in toluene in a glass vial. Then, the needed amount of oligomer was added. The vial was sealed and stirred gently (by means of a Teflon-coated magnetic stirrer) at room temperature for 2 days. Subsequently, the toluene was evaporated in a hood at room temperature for 8 days. Finally, the solutions were put under vacuum for 2 days at 150 °C in order to strip residual amounts of toluene. The key molecular characteristics of the two solutions are listed in Table 1. The number of entanglements per chain (Z) is calculated as the ratio between M_w and the entanglement molar mass (M_e). To be consistent with earlier works (Huang et al. 2015; Costanzo et al. 2016), we used a M_e value of 13.3 kg/mol as reported for atactic polystyrene (Fetters et al. 2006; Huang et al. 2013a, b). The plateau moduli of Table 1 are determined from the linear viscoelastic response as the values of G' at the minimum of the loss factor. Such values are close to those obtained according to the theoretical prediction, $G_N^0(\phi) = G_N^0(1)\phi^{1+\alpha}$, where $G_N^0(\phi)$ is the plateau modulus of the solution, $G_N^0(1)$ is the plateau modulus of the melt, and α is the dilution exponent (here taken to be equal to 1) (Rubinstein and Colby 2003; Graessley 2008; Huang et al. 2013a; Huang et al. 2015). These values of $G_N^0(\phi)$ were chosen in order to prevent normal force transducer overload when $\dot{\gamma}$ approaches values corresponding to frequencies in the plateau region of G'.

Modeling

We will here use the model proposed in our previous paper (Costanzo et al. 2016), with a simplification due to the fact that in shear flows, the monomeric friction coefficient essentially remains at the equilibrium value, differently from extensional flows where chains co-align considerably, yielding anisotropic friction. Furthermore, we will neglect the effect of convective constraint release (CCR) previously shown to play a negligible role in

Table 1 Molecular parameters of the two PS solutions

	ϕ	Z	T_{ref} (°C)	G_N^0 (Pa)	τ_d (s)	τ_R (s)
PS200k-2k-50	0.5	7.5	130	4.2×10^4	5.56	0.944
PS545k-2k-70	0.7	28.7	170	8.5×10^4	5.27	0.136

ϕ is the polymer weight fraction, Z is the number of entanglements per chain, T_{ref} is the reference temperature at which relaxation times are evaluated (the same temperature was used for nonlinear measurements), G_N^0 is the entanglement plateau modulus determined as G' at the minimum of $\tan(\delta)$, τ_d is the terminal relaxation time determined from Eq. (12), and τ_R is the Rouse time determined from $\tau_R = Z^2 \tau_e$ with τ_e as the Rouse time of the entangled subchain, estimated from the Baumgartel-Schausberger-Winter (BSW) fit of the linear frequency response

sheared PS systems (Costanzo et al. 2016). As a consequence, in the nonlinear range, the relaxation times of the linear viscoelastic (LVE) spectrum do not change, and the stress tensor (σ) can be written as the following sum over modes:

$$\sigma(t) = C_Q \lambda^2(t) \frac{f(\lambda)}{f_0} \sum \frac{G_i}{\tau_i} \int_{-\infty}^{t} dt' \exp\left(-\frac{t-t'}{\tau_i}\right) Q\left[E(t,t')\right] \quad (7)$$

where $\{G_i, \tau_i\}$ is the discrete Maxwell set of LVE moduli and relaxation times, tensor E is the deformation gradient between past time (t') and current time (t), and Q is the Doi-Edwards tensor, here replaced (for simplicity) by the following unit-trace Seth-type measure

$$Q = \frac{B^q}{tr B^q} \quad (8)$$

based on the Finger tensor $B = E^T \cdot E$. Several choices for the exponent q have been made, from $q = 1$ (Larson 1984) to $q = 1/2$ (Marrucci et al. 2000; Costanzo et al. 2016) or $q = 1/3$ (Ianniruberto 2015; Park and Ianniruberto 2017). The latter value, $q = 1/3$, will be adopted here, implying slightly less affine orientation. The scalar coefficient C_Q is Q-dependent (and is equal to $3/q$ for the Seth-type tensors of Eq. (8)) and is needed for Eq. (7) to properly reduce to the multimode Maxwell-like LVE limit; λ is the stretch ratio of the entangled subchain, and $f(\lambda)$ is the force factor that accounts for the non-Gaussian behavior of subchains

$$f(\lambda) = \frac{\mathscr{L}^{-1}(\lambda/\lambda_{max})}{3\lambda/\lambda_{max}}, \quad \lambda_{max} = a/b. \quad (9)$$

In Eq. (9), $\mathscr{L}^{-1}$ is the inverse Langevin function, b = 18Å is PS Kuhn length (Rubinstein and Colby 2003), and a is the tube diameter, changing with dilution according to $a(\phi) = a(1)\phi^{-1/2}$, where the tube diameter of PS melts is given (in Å) by $a(1) = 85(3f_0/C_Q)^{1/2}$ (Ianniruberto 2015), with f_0 as the equilibrium value of f. (In PS melts, a is not much larger than b; hence, even for $\lambda = 1$, i.e., at equilibrium, f_0 comes out slightly larger than unity.)

There remains to specify how λ varies with time. In line with the suggestion of Costanzo et al. (2016), we will assume that in a shear flow with a shear rate $\dot{\gamma}$, the stretch ratio obeys the differential equation (x and y being the shear and gradient directions, respectively)

$$\frac{d\lambda}{dt} = \dot{\gamma} S_{xy} \varphi \lambda - \frac{f\lambda - f_0}{\tau_R}, \quad S_{xy} = \frac{1}{\tau_d} \int_{-\infty}^{t} dt' \exp\left(-\frac{t-t'}{\tau_d}\right) Q_{xy}\left[\gamma(t,t')\right]. \quad (10)$$

Table 2 Parameters of the multimode Maxwell fit for the two PS solutions

Parameters	Values								
PS200k-2k-50									
τ_i (s)	2.44×10^1	3.92	6.30×10^{-1}	1.01×10^{-1}	1.36×10^{-2}	2.62×10^{-3}	4.22×10^{-4}	6.79×10^{-5}	1.09×10^{-5}
G_i (Pa)	4.36×10^2	1.92×10^4	1.93×10^4	2.01×10^4	3.53×10^4	1.04×10^5	2.81×10^4	3.94×10^6	4.60×10^3
PS545k-2k-70									
τ_i (s)	5.97	6.91×10^{-1}	7.99×10^{-2}	9.25×10^{-3}	1.07×10^{-3}	1.24×10^{-4}	1.43×10^{-5}	1.66×10^{-6}	1.92×10^{-7}
G_i (Pa)	2.39×10^4	2.81×10^4	2.32×10^4	2.03×10^4	2.81×10^4	9.37×10^4	2.11×10^5	2.41×10^6	8.82×10^6

Here, τ_R is the Rouse time of the polymer chain, and the tumbling function $\varphi(t)$, inspired by the work of Khomami and co-workers (Nafar Sefiddashti et al. 2015), is given by

$$\varphi(t) = \cos(2\pi\omega t)\exp(-\beta t), \quad \omega = \frac{Wi_R^{-0.2}}{8\pi}\dot{\gamma}, \quad \beta = \frac{Wi_R^{-0.2}}{8}\dot{\gamma} \tag{11}$$

where $Wi_R = \dot{\gamma}\tau_R$ is the Weissenberg number based on the Rouse time. Finally, the disengagement (terminal) time (τ_d) controlling the evolution of the average xy-orientation (S_{xy}) of the entanglement tube is calculated from the LVE spectrum through the classical formula (Ferry 1980)

$$\tau_d = \frac{\sum_i G_i \tau_i^2}{\sum_i G_i \tau_i} \tag{12}$$

The model Eqs. (7)–(12) are solved by using the estimated Rouse time values reported in Table 1 and the LVE Maxwell spectrum $\{G_i, \tau_i\}$ of Table 2 (see the next section).

Results and discussion

Figure 4 shows the LVE master curves of the two PS solutions at the respective reference temperatures of 130 °C (PS200k-2k-50) and 170 °C (PS545k-2k-70). Nonlinear transient shear experiments have been performed at the same temperatures, as mentioned in Table 1. We note that, due to the different reference temperatures, the terminal relaxation times of the two solutions are nearly the same (see Table 1), while the plateau of PS545k-2k-70 extends for several decades in frequency, allowing to span a larger portion of the rubber-like region. The high-frequency crossover is not the same for the two solutions, indicating different entanglement numbers and glass transition temperatures due to the different fractions of solvent.

Both master curves were fitted with a multimode Maxwell model by using the Reptate software (http://reptate.com/). The corresponding values of the set $\{G_i, \tau_i\}$ are listed in Table 2 and used for the model predictions of the nonlinear response. The discrete spectra of Table 2 will also be used in conjunction with Eq. (13)

below for the first normal stress coefficient ($\Psi_1 = \Psi_1(t)$) of the rubber-like liquid constitutive equation (Lodge and Meissner 1973)

Similar to what has been done in our previous work (Costanzo et al. 2016), the LVE master curves of the samples were also fitted with the BSW relaxation model in order to estimate the Rouse time τ_e of the entangled subchain and hence the chain Rouse time τ_R reported in Table 1.

Figure 5 depicts the data from dynamic frequency sweep tests performed on different samples of PS200k-2k-50 at 130 °C. Two samples were measured with the 6-mm partition, and two more with the 10-mm partition. The dynamic moduli obtained with different loadings are in excellent agreement with one another. This confirms the excellent reproducibility of the loadings and the high reliability of the present method for testing different samples. In general, we note that, if the CPP geometry is used correctly, the reproducibility of rheological measurements is as good as that obtained with standard geometries.

Concerning nonlinear measurements, we prepared a series of identical samples for each solution by means of vacuum compression molding (Costanzo et al. 2016). The mass (m) of the samples was between 46 and 47 mg, so that the outer
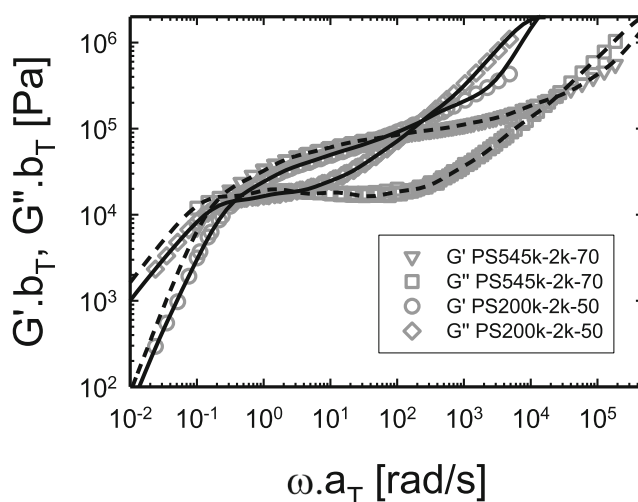

Fig. 4 LVE master curves of the two PS solutions. PS200k-2k-50 at a reference temperature (T_{ref}) of 130 °C and PS545k-2k-70 at a T_{ref} of 170 °C. Lines represent multimode Maxwell fits to the data using the Reptate software
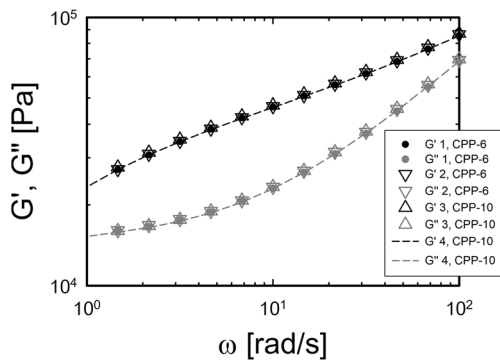
Fig. 5 Reproducibility of the loadings. Dynamic frequency sweep tests of different samples performed with four different loadings of PS200k-2k-50: two with CPP-6 and two with CPP-10

radius value (R) was equal to 6.04 ± 0.05 mm, according to Eq. (4). We point out that having identical samples is not a necessary condition for applying Eqs. (5)–(6). Indeed, the requirement for measuring N_1 and N_2 with two measuring partitions is the knowledge of the outer radius of the sample and that of the measured inner partition in two independent measurements. However, having identical samples allows for direct comparison of the apparent normal force signals. Moreover, from a practical standpoint, the preparation of multiple samples can be easily done at once by using a drilled platen with identical holes placed in a hot press. After preparation, we loaded the samples onto the ARES rheometer equipped with the CPP, and performed transient start-up tests at selected shear rates. Figure 6 depicts different start-up and relaxation (the latter not further discussed here) shear tests performed on the solution PS200k-2k-50 at 130 °C and $\dot{\gamma} = 6$ s^{-1}. In order to demonstrate the reproducibility of the results with the two different partitions, we report two different loadings for each partition, CPP-6 and CPP-10.

In Fig. 6a, we can observe the high reproducibility of the transient viscosity of the two different samples in the two different geometries. The undershoot before steady state is thought to be a signature of tumbling (Costanzo et al. 2016). In Fig. 6b, the apparent normal force signals corresponding to the start-up tests of fig. 6a are reported. The apparent normal stress acting on the CPP-6 partition is different from that acting on the CPP-10 one, as expected. In addition, we note that, differently from the transient viscosity, no undershoot following the overshoot is detectable in the transient $N_{app,1}$. This is in agreement with recent reports on nonlinear shear rheology of molten polymers (Costanzo et al. 2016; Stephanou et al. 2017). Transient normal force signals in Fig. 6b are affected by noise and axial compliance at early times; therefore, we limit our analysis to the steady state. Also in the steady state, a neat separation between the values of $N_{app,1}$ with 6 mm and $N_{app,2}$ with 10 mm is found. We note that the steady-state values of normal force are well above the experimental noise, which can be observed in the late stages of the relaxation of the signals of N_{app}. The steady-state

values of $N_{app,1}$ and $N_{app,2}$ from Fig. 6b are then inserted into Eqs. (5)–(6) in order to obtain the true steady-state values of N_1 and N_2. From the latter, we obtain Ψ_1 and Ψ_2 by dividing both N_1 and N_2 by $\dot{\gamma}^2$. The steady-state values of η, Ψ_1, and Ψ_2 are reported for the two PS solutions in Fig. 7, with η as a function of $1/\dot{\gamma}$ and Ψ_1 and Ψ_2 as a function of $k/\dot{\gamma}$ (with $k = 2.2$). In Fig. 7, we also report the LVE envelope for the transient viscosity and the Lodge-Meissner prediction for Ψ_1 as a function of time.

Specifically, the LVE envelope was obtained from the complex viscosity by using a combination of the Cox-Merz rule (Cox and Merz 1958), $\eta(\dot{\gamma}) = \eta(\omega)|_{\omega=\dot{\gamma}}$ with the Gleissle relationship (Gleissle 1980), $\eta^+(t) = \eta(\dot{\gamma})|_{\dot{\gamma}=1/t}$. The curve of $\Psi_1(t)_{RTS}$ was calculated from the following equation (Lodge and Meissner 1973; Graessley 2008):

$$\Psi_1(t)_{RTS} = 2 \sum_{i=1}^{n} \tau_i^2 G_i \left[1 - \left(1 + \frac{t}{\tau_i} \right) \exp\left(-\frac{t}{\tau_i} \right) \right] \quad (13)$$

by using the relaxation spectrum $\{G_i, \tau_i\}$ reported in Table 2 (RTS stands for relaxation time spectrum). Figure 7 shows that the Cox-Merz and Gleissle rules work very well in predicting the nonlinear shear viscosity, while the Lodge-Meissner prediction is off by a factor of about 2 in the time scale. Previous results on N_2 reported in the literature suggest that its value is negative and
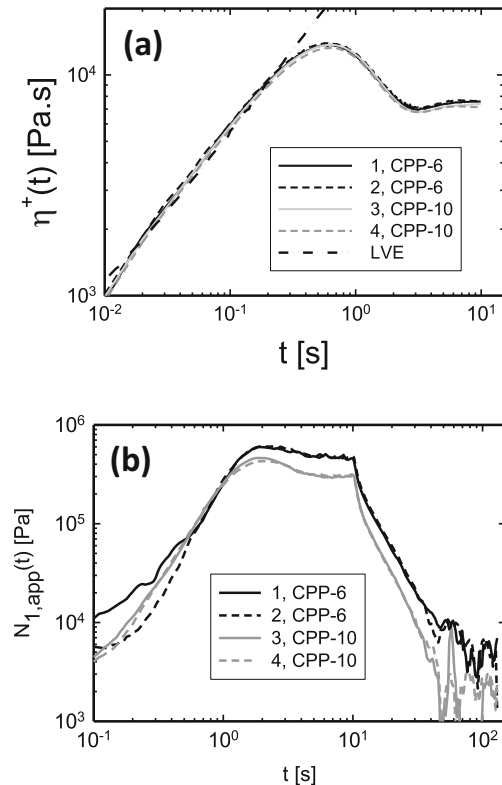

Fig. 6 Transient shear data of the entangled polystyrene solution PS200k-2k-50 at 130 °C and $\dot{\gamma} = 6$ s^{-1} for four different loadings: two samples with CPP-6 and two samples with CPP-10. **a** Start-up viscosity. **b** Start-up and relaxation of the apparent normal stress

much lower compared to that of N_1 (Bird et al. 1977; Doi and Edwards 1986; Tanner 2000), as indeed shown by our data as well.

The complete set of shear start-up viscosity data is reported in Fig. 8 for the two PS solutions, along with the predictions of the model. Notice that the data encompass several samples (loadings) and both CPP fixtures. Model predictions agree reasonably well with both datasets.

Figure 9 reports the steady-state values of viscosity and normal stress differences of the two solutions. For the PS200k-2k-50 solution, predictions agree well with data, while for PS545k-2k-70, the normal stress differences are somewhat overestimated. Whereas more work is needed to properly assess this difference, it is tempting to think of possible flow-induced disentanglement which is more relevant for larger number of entanglements and is not considered in the model.

Finally, the measured ratio $-N_2/N_1$ is reported in Fig. 10 for both solutions as a function of the orientational (terminal) Weissenberg number $Wi_d = \dot\gamma \tau_d$. With the exception of a single data point, model predictions appear to agree with data very well, although the uncertainty shown by the error bars is certainly quite large. Within the uncertainty, data appear to indicate larger values of the ratio for the PS200k-2k-50 solution with respect to PS545k-2k-70. The same ordering is found, though marginally, in the model predictions. We believe that this is due to the different LVE spectra of the two
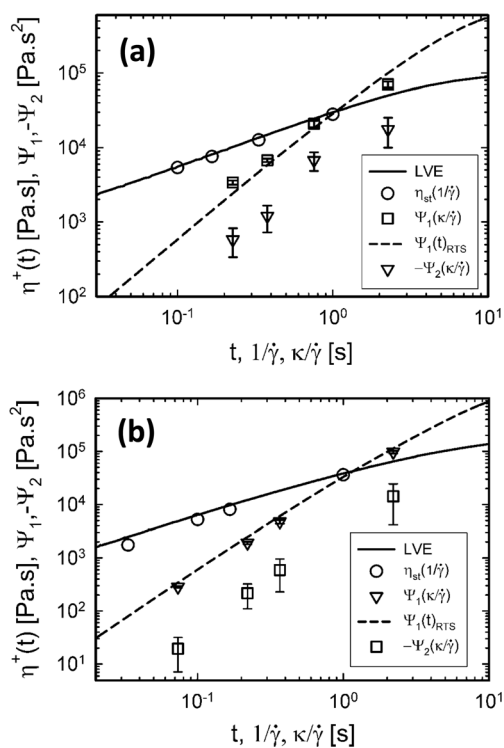
samples (see also Table 2), with the ratio $-N_2/N_1$ decreasing (at fixed Wi_d) when the spectrum approaches the single-mode limit (lower curve in Fig. 10). Indeed, the PS545k-2k-70 solution is more entangled than PS200k-2k-50, hence it is closer to the single-mode Maxwell limit in the terminal regime.

It should be noted that very similar values of the normal stress ratio dropping from nearly 0.3 to nearly 0.1 with increasing shear rate were also reported in previous studies on PS 200 kg/mol melts at 175 °C, using CPP and different sample radii in a range of Wi_d from approximately 0.1 to 40 (Schweizer et al. 2004). Similar results were reported long ago (Gao et al. 1981) for solutions of high-molar-mass PS (M_w between 200 and 2000 kg/mol) in n-butylbenzene at the fixed PS concentration of 450 kg/m³ and temperature of 25 °C (corresponding to $\phi = 0.52$ w/w), using flush-mounted transducers. The latter technique was also used by Magda and Baek (1994) to demonstrate the shear thinning of $-N_2/N_1$ of PS solutions in dioctyl phthalate. Analysis of step-strain experiments yielded essentially the same behavior (Brown et al. 1995; Olson et al. 1998). The shear thinning of the $-N_2/N_1$ ratio for polymer melts was investigated by means of coarse-grained non-equilibrium molecular dynamics simulations (Padding and Briels 2003), as well as by Brownian simulations based on the slip-link model (Cao 2011; Delbiondo et al. 2013). In the former case, the

Fig. 7 Viscometric steady-state functions of the two PS solutions here investigated. **a** PS200k-2k-50, **b** PS545k-2k-70. The value of κ is 2.2 in both cases. Error bars for N_1 are at most the size of the symbols while for N_2, the error is larger
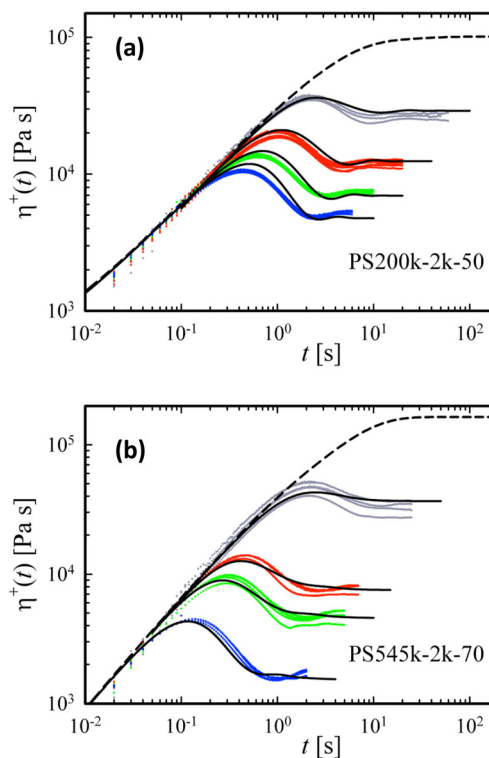

Fig. 8 Shear start-up viscosity curves for **a** PS200k-2k-50 and **b** PS545k-2k-70. Dots (merging into continuous lines at long times) are data from repeated runs at each shear rate (different samples and two CPPs). Dashed and solid black lines are LVE and nonlinear model predictions, respectively. Shear rates are as follows: **a** 1, 3, 6, and 10 s⁻¹ and **b** 1, 6, 10, and 30 s⁻¹, from top to bottom
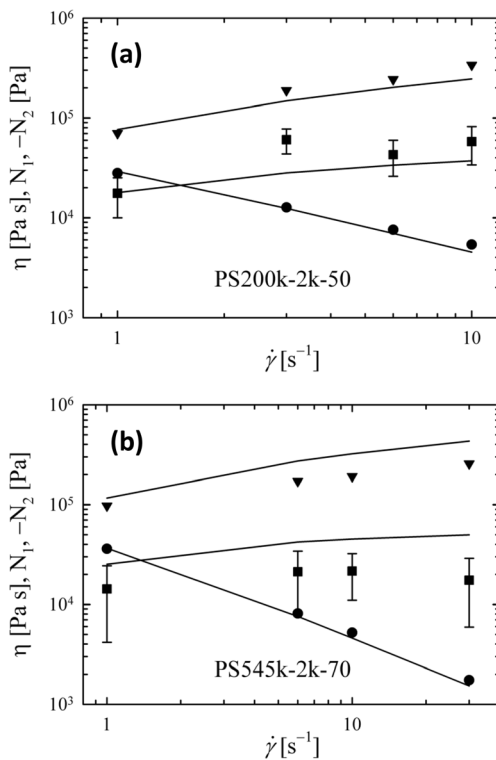
Fig. 9 **a**, **b** Measured steady-state values of shear viscosity (circles) and the first (triangles) and second (squares) normal stress differences vs. shear rate. Error bars for η and N_1 are within the size of the symbols. Lines are model predictions
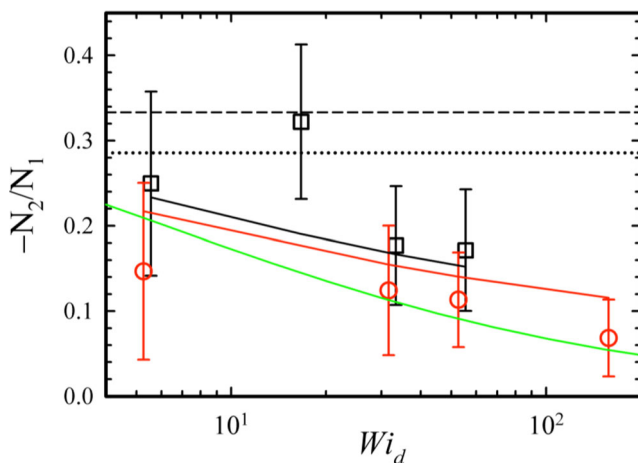

Fig. 10 Steady-state values of the normal stress ratio ($-N_2/N_1$) vs. the Weissenberg number (Wi_d). Black squares and red circles are data for PS200k-2k-50 and PS545k-2k-70, respectively. Black and red solid lines are the corresponding model predictions. Within the uncertainties, the normal stress ratio roughly decreases from 0.3 to 0.1 with Wi_d increasing from about 5 to almost 200. Dotted and dashed lines indicate the asymptotic values of the normal stress ratio for vanishing shear rates predicted by the $\boldsymbol{Q}$ tensor with the independent alignment approximation (IAA) of Doi and Edwards and by that used here, 2/7 and 1/3, respectively. The lowest curve (green) is the single-mode prediction (with the 1/3 $\boldsymbol{Q}$ tensor used here)

normal stress ratio varied from 0.12 at a rate of 100 μs^{-1} to 0.046 at 3000 μs^{-1} (terminal time (τ_d) = 0.025 μs; hence, $Wi_d = \dot{\gamma}\tau_d$ comprised between 2.5 and 75) whereas in the latter case, a higher value was reported for the zero-shear limit (0.4). Using a consistently unconstrained Brownian slip-link model, Schieber et al. (2007) found smaller values (below 0.2). Similarly, by using non-equilibrium molecular dynamics (NEMD) simulations, Baig and co-workers found that the ratio $-N_2/N_1$ for a polyethylene melt decreases from 0.2 to approximately 0.1 by increasing the Weissenberg number from 10 to 10^4 (Baig et al. 2010). NEMD simulations were also performed by Xu et al. (2014) on linear polymer melts in both the unentangled and entangled regimes. They found that, in strong shear flows, the normal stress differences of well-entangled linear polymers follow the power laws $N_1 \sim \dot{\gamma}^{2/3}$ and $-N_2 \sim \dot{\gamma}^{0.82}$, in contrast with the thinning behavior of the normal stress ratio. We also note that Aoyagi and Doi (2000) reported results of large-scale molecular dynamics simulations yielding a ratio between 0.1 and almost zero when the shear rate ranged from about 3×10^{-5} s^{-1} to about 10^{-2} s^{-1}.

A final comment on the modeling is in the order: the first molecular theory for entangled polymers explicitly predicting a nonzero second normal stress difference is the integral model of Doi and Edwards (1979), to which also the model adopted here reduces in the no-chain-stretch limit ($\lambda = 1$) of the steady state. Conversely, molecular models of the differential type usually predict a zero second normal stress difference, even in the highly sophisticated version of the GLaMM model (Graham et al. 2003), due to the decoupling approximation used in the calculation of the tube tangent correlation function.

Conclusions

We have developed and tested a simple methodology for measuring both N_1 and N_2 in entangled polymers at elevated temperatures by means of a modular CPP geometry, and further assessed the data by means of modeling predictions. Our CPP setup is implemented on the ARES rheometer but can be also implemented on MCR 702 with appropriate modifications. Reliable measurements of the three viscometric functions (η, N_1, N_2) are reported, with a small amount of samples and excellent thermal stability at high temperatures. Within the limitations imposed by the maximum axial force of the transducer, N_1 and N_2 data are obtained over a Weissenberg number range covering nearly two decades. The obtained data for entangled polystyrene solutions in oligostyrene were compared well with literature data (albeit at room temperature) and with theoretical predictions based on the nonlinear model explicitly including the effect of molecular tumbling (Costanzo et al. 2016). Despite limitations, which are

discussed and provide motivation for improvements, the present results are promising and may trigger further investigations of nonlinear shear rheology of highly elastic samples at elevated temperatures.

References

Adams N, Lodge AS (1964) Rheological properties of concentrated polymer solutions II. A cone-and-plate and parallel-plate pressure distribution apparatus for determining normal stress differences in steady shear flow. Phil Trans R Soc London A 256:149–184

Alcoutlabi M, Baek SG, Magda JJ, Shi X, Hutcheson SA, McKenna GB (2009) A comparison of three different methods for measuring both normal stress differences of viscoelastic liquids in torsional rheometers. Rheol Acta 48:191–200. https://doi.org/10.1007/s00397-008-0330-z

Aoyagi T, Doi M (2000) Molecular dynamics simulation of entangled polymers in shear flow. Comput Theor Polym Sci 10:317–321. https://doi.org/10.1016/S1089-3156(99)00041-0

Baek S, Magda JJ (2003) Monolithic rheometer plate fabricated using silicon micromachining technology and containing miniature pressure sensors for N1 and N2 measurements. J Rheol 47:1249–1260. https://doi.org/10.1122/1.1595095

Baig C, Mavrantzas VG, Kröger M (2010) Flow effects on melt structure and entanglement network of linear polymers: results from a non-equilibrium molecular dynamics simulation study of a polyethylene melt in steady shear. Macromolecules 43:6886–6902. https://doi.org/10.1021/ma100826u

Baird DG (1975) A possible method for determining normal stress differences from hole pressure error data. Trans Soc Rheol 19:147–151. https://doi.org/10.1122/1.549392

Barnes AH, Eastwood AR, Yates B (1975) A comparison of the rheology of two polymeric and two micellar systems. Part II: second normal stress difference. Rheol Acta 14:61–70

Bird RB, Armstrong RC, Hassager O (1977) Dynamics of polymer liquids. Volume 1. Fluid mechanics. Wiley, New York

Boger DV, Denn MM (1980) Capillary and slit methods of normal stress measurements. J Nonnewton Fluid Mech 6:163–185. https://doi.org/10.1016/0377-0257(80)80001-2

Boger D V, Walters K (1993) Rheological phenomena in focus. Vol. 4, 1st edn. Amsterdam

Brown EF, Burghardt WR, Kahvand H, Venerus DC (1995) Comparison of optical and mechanical measurements of second normal stress difference relaxation following step strain. Rheol Acta 34:221–234

Cao J (2011) Molecular dynamics study of polymer melts. University of Reading

Carotenuto C, Vananroye A, Vermant J, Minale M (2015) Predicting the apparent wall slip when using roughened geometries: a porous medium approach. J Rheol 59:1131–1149. https://doi.org/10.1122/1.4923405

Christiansen EB, Leppard WR (1974) Steady-state and oscillatory flow properties of polymer solutions. J Rheol 18:65–86. https://doi.org/10.1122/1.549327

Costanzo S, Huang Q, Ianniruberto G, Marrucci G, Hassager O, Vlassopoulos D (2016) Shear and extensional rheology of polystyrene melts and solutions with the same number of entanglements. Macromolecules 49:3925–3935. https://doi.org/10.1021/acs.macromol.6b00409

Couturier É, Boyer F, Pouliquen O, Guazzelli É (2011) Suspensions in a tilted trough: second normal stress difference. J Fluid Mech 686:26–39. https://doi.org/10.1017/jfm.2011.315

Cox WP, Merz EH (1958) Correlation of dynamic and steady flow viscosities. J Polym Sci 28:619–622

Crawley RL and Graessley WW (1977) Geometry effects on stress transient data obtained by cone and plate flow. Trans Soc Rheol 21(1):19-49. https://doi.org/10.1122/1.549462

Cwalina CD, Wagner NJ (2014) Material properties of the shear-thickened state in concentrated near hard-sphere colloidal dispersions. J Rheol 58:949–967

Delbiondo D, Masnada E, Merabia S et al (2013) Numerical study of a slip-link model for polymer melts and nanocomposites. J Soft Cond Matt 138:194902. https://doi.org/10.1063/1.4799263

Doi M, Edwards SF (1979) Dynamics of concentrated polymer systems. Part 4.—Rheological properties. J Chem Soc, Faraday Trans 2 75:38-54

Doi M, Edwards SF (1986) The theory of polymer dynamics. Oxford Scientific Publications, New York

Eggers H, Schümmer P (1994) A new method for determination of normal stress differences in highly visco-elastic substances using a modified Weissenberg rheometer. J Rheol 38:1169–1177

Ferry JD (1980) Viscoelastic Properties of Polymers. Wiley, New York

Fetters LJ, Lohse DJ, Colby RH (2006) Chapter 25 chain dimensions and entanglement spacings. Phys Prop Polym Handb:445–452. https://doi.org/10.1007/978-0-387-69002-5

Gamonpilas C, Morris JF, Denn MM (2016) Shear and normal stress measurements in non-Brownian monodisperse and bidisperse suspensions. J Rheol 60:289–296. https://doi.org/10.1122/1.4942230

Gao HW, Ramachandran S, Christiansen EE (1981) Dependency of the steady-state and transient viscosity and first and second normal stress difference functions on molecular weight for linear mono and polydisperse polystyrene solutions. J Rheol 25:213–235

Ginn RF, Metzner AB (1969) Measurements of stresses developed in steady laminar shearing flows of viscoelastic media. Trans Soc Rheol 13:429–453

Gleissle W (1980) Two simple time-shear rate relations combining viscosity and first normal stress coefficient in the linear and non-linear flow range. In: Astarita G, Marrucci G, Nicolais L (eds) Rheology, vol 2. Plenum, New York, pp 457–462

Graessley WW (2008) Polymeric liquids and networks: dynamics and rheology. Garland Science, London

Graham RS, Likhtman AE, McLeish TCB, Milner ST (2003) Microscopic theory of linear, entangled polymer chains under rapid deformation including chain stretch and convective constraint release. J Rheol 47:1171–1200. https://doi.org/10.1122/1.1595099

Hansen MG, Nazem F (1975) Transient normal force transducer response in a modified Weissenberg rheogoniometer. Trans Soc Rheol 19:21–36. https://doi.org/10.1122/1.549388

Harris J (1968) Measurement of normal stress differences in solutions of macromolecules. Nature 217:1248–1249

Hemingway EJ, Kusumaatmaja H, Fielding SM (2017) Edge fracture in complex fluids. Phys Rev Lett 119:028006(5). https://doi.org/10.1103/PhysRevLett.119.028006

Higashitani K, Pritchard WG (1972) A kinematic calculation of intrinsic errors in pressure measurements made with holes. Trans Soc Rheol 16:687–696. https://doi.org/10.1122/1.549270

Huang Q, Alvarez NJ, Matsumiya Y, Rasmussen HK, Watanabe H, Hassager O (2013a) Extensional rheology of entangled polystyrene solutions suggests importance of nematic interactions. ACS Macro Lett 2:741–744. https://doi.org/10.1021/mz400319v

Huang Q, Hengeller L, Alvarez NJ, Hassager O (2015) Bridging the gap between polymer melts and solutions in extensional rheology. Macromolecules 48:4158–4163. https://doi.org/10.1021/acs.macromol.5b00849

Huang Q, Mednova O, Rasmussen HK, et al (2013b) Concentrated polymer solutions are different from melts: role of entanglement molecular weight. Macromolecules 46:5026–5035. https://doi.org/10.1021/ma4008434

Ianniruberto G (2015) Quantitative appraisal of a new CCR model for entangled linear polymers. J Rheol 59:211–235. https://doi.org/10.1122/1.4903495

Jackson R, Kaye A (1966) The measurement of the normal stress differences in a liquid undergoing simple shear flow using a cone-and-plate total thrust apparatus. J Appl Phys 17:1355–1360

Kalogrianitis SG, van Egmond JW (1997) Full tensor optical rheometry of polymer fluids. J Rheol 41:343–364. https://doi.org/10.1122/1.550806

Kasehagen LJ, Macosko CW (1998) Nonlinear shear and extensional rheology of long-chain randomly branched polybutadiene. J Rheol 42:1303–1327. https://doi.org/10.1122/1.550892

Kearsley EA (1973) Measurement of normal stress by means of hole pressure. Trans Soc Rheol 17:617–628. https://doi.org/10.1122/1.549311

Keentok M, Georgescu AG, Sherwood AA, Tanner RI (1980) The measurement of the second normal stress difference for some polymer solutions. J Nonnewton Fluid Mech 6:303–324. https://doi.org/10.1016/0377-0257(80)80008-5

Keentok M, Xue SC (1999) Edge fracture in cone-plate and parallel plate flows. Rheol Acta 38:321–348

Kotaka T, Kurata M, Tamura M (1959) Normal stress effect in polymer solutions. J Appl Phys 30:1705–1712. https://doi.org/10.1063/1.1735041

Kulicke WM, Wallbaum U (1985) Determination of first and second normal stress differences in polymer solutions in steady shear flow and limitations caused by flow irregularities. Chem Eng Sci 40:961–972. https://doi.org/10.1016/0009-2509(85)85009-0

Kuo Y, Tanner RI (1972) Laminar Newtonian flow in open channels with surface tension. Int J Mech Sci 14:861–873

Kuo Y, Tanner RI (1974) On the use of open-channel flows to measure the second normal stress difference. Rheol Acta 13:443–456. https://doi.org/10.1007/BF01521740

Larson RG (1984) A constitutive equation for polymer melts based on partially extending strand convection. J Rheol 28:545–571. https://doi.org/10.1122/1.549761

Lee J-Y, Magda JJ, Hu H, Larson RG (2002) Cone angle effects, radial pressure profile, and second normal stress difference for shear-thickening wormlike micelles. J Rheol 46:195–208. https://doi.org/10.1122/1.1428319

Lodge AS (1964) Elastic liquids: an introductory vector treatment of finite strain polymer rheology. Academic Press, London

Lodge AS (1993) Normal stress differences from hole pressure measurements. In: Collyer AA, Clegg DW (eds) Rheological measurement. Springer, Dordrecht, pp 345–382

Lodge AS, Meissner J (1973) Comparison of network theory predictions with stress/time data in shear and elongation for a low-density polyethylene melt. Rheol Acta 12:41–47

Macosko CW (1994) Rheology: principles, measurements and applications. Whiley VCH, New York

Magda JJ, Baek SG (1994) Concentrated entangled and semidilute entangled polystyrene solutions and the second normal stress difference. Polymer (Guildf) 35:1187–1194. https://doi.org/10.1016/0032-3861(94)90010-8

Magda JJ, Baek SG, DeVries KL, Larson RG (1991) Shear flows of liquid crystal polymers: measurements of the second normal stress difference and the Doi molecular theory. Macromolecules 24:4460–4468. https://doi.org/10.1021/ma00015a034

Marrucci G, Greco F, Ianniruberto G (2000) Simple strain measure for entangled polymers. J Rheol 44:845–854. https://doi.org/10.1122/1.551124

Marsh BD, Pearson JRA (1968) The measurement of normal-stress differences using a cone-and-plate total thrust apparatus. Rheol Acta 4:326–331

Meissner J.(1972) Modifications of the Weissenberg Rheogoniometer for Measurement of Transient Rheological Properties of Molten Polyethylene under shear. Comparison with Tensile Data. J Appl Polym Sci 16(11);2877-2899. https://doi.org/10.1002/app.1972.070161114

Meissner J, Garbella RW, Hostettler J (1989) Measuring normal stress differences in polymer melt shear flow. J Rheol 33:843–864

Miller E, Rothstein JP (2004) Control of the sharkskin instability in the extrusion of polymer melts using induced temperature gradients. Rheol Acta 44:160–173

Nafar Sefiddashti MH, Edwards BJ, Khomami B (2015) Individual chain dynamics of a polyethylene melt undergoing steady shear flow. J Rheol 59(1):119-153. https://doi.org/10.1122/1.4903498

Nafar Sefiddashti MH, Edwards BJ, Khomami B (2015) Individual chain dynamics of a polyethylene melt undergoing steady shear flow. J Rheol 59:119–153. https://doi.org/10.1122/1.4903498

Ohl N, Gleissle W (1992) The second normal stress difference for pure and highly filled viscoelastic fluids. Rheol Acta 31:294–305

Olson DJ, Brown EF, Burghardt WR (1998) Second normal stress difference relaxation in a linear polymer melt following step-strain. J Polym Sci Part B Polym Phys 36:2671–2675. https://doi.org/10.1002/(SICI)1099-0488(199810)36:14<2671::AID-POLB20>3.0.CO;2-7

Padding JT, Briels WJ (2003) Coarse-grained molecular dynamics simulations of polymer melts in transient and steady shear flow. J Chem Phys 118:10276–10286. https://doi.org/10.1063/1.1572459

Park GW, Ianniruberto G (2017) Flow-induced nematic interaction and friction reduction successfully describe PS melt and solution data in extension startup and relaxation. Macromolecules 50:4787–4796. https://doi.org/10.1021/acs.macromol.7b00208

Pollett WFO (1955) Rheological behaviour of continuously sheared polythene. Br J Appl Phys 6:199–206

Pollett WFO, Cross AH (1950) A continuous-shear rheometer for measuring total stresses in rubber-like materials. J Sci Instrum 27:209–212

Pritchard WG (1971) Measurements of the viscometric functions for a fluid in steady shear flows. Philos Trans R Soc London A Math Phys Eng Sci 270:507–556. https://doi.org/10.1098/rsta.1971.0088

Ravindranath S, Wang S-Q (2008) Steady-state measurements in stress plateau region of entangled polymer solutions: controlled-rate and controlled-stress modes. J Rheol 52:957–980

Rubinstein M, Colby RH (2003) Polymer physics. Oxford University Press, Oxford

Savins JG, Metzner AB (1970) Radial (secondary) flows in rheogoniometric devices. Rheol Acta 9:365–373

Schieber JD, Nair DM, Kitkrailard T (2007) Comprehensive comparisons with nonlinear flow data of a consistently unconstrained Brownian slip-link model. J Rheol 51:1111–1141. https://doi.org/10.1122/1.2790460

Schweizer T (2002) Measurement of the first and second normal stress differences in a polystyrene melt with a cone and partitioned plate tool. Rheol Acta 41:337–344. https://doi.org/10.1007/s00397-002-0232-4

Schweizer T, Bardow A (2006) The role of instrument compliance in normal force measurements of polymer melts. Rheol Acta 45:393–402. https://doi.org/10.1007/s00397-005-0056-0

Schweizer T, Hostettler J, Mettler F (2008) A shear rheometer for measuring shear stress and both normal stress differences in polymer melts simultaneously: the MTR 25. Rheol Acta 47:943–957

Schweizer T, Schmidheiny W (2013) A cone-partitioned plate rheometer cell with three partitions (CPP3) to determine shear stress and both normal stress differences for small quantities of polymeric fluids. J Rheol 57:841–856. https://doi.org/10.1122/1.4797458

Schweizer T, Stöckli M (2008) Departure from linear velocity profile at the surface of polystyrene melts during shear in cone-plate geometry. J Rheol 52:713–727. https://doi.org/10.1122/1.2896110

Schweizer T, van Meerveld J, Öttinger HC (2004) Nonlinear shear rheology of polystyrene melt with narrow molecular weight distribution—experiment and theory. J Rheol 48:1345–1363. https://doi.org/10.1122/1.1803577

Sing A, Nott PR (2003) Experimental measurements of the normal stresses in sheared Stokesian suspensions. J Fluid Mech 490:293–320. https://doi.org/10.1017/S0022112003005366

Skorski S, Olmsted PD (2011) Loss of solutions in shear banding fluids driven by second normal stress differences. J Rheol 55:1219–1246. https://doi.org/10.1122/1.3621521

Snijkers F, Vlassopoulos D (2011) Cone-partitioned-plate geometry for the ARES rheometer with temperature control. J Rheol 55:1167–1186. https://doi.org/10.1122/1.3625559

Stephanou PS, Schweizer T, Kröger M (2017) Communication: appearance of undershoots in start-up shear: experimental findings captured by tumbling-snake dynamics. J Chem Phys 146:161101. https://doi.org/10.1063/1.4982228

Sturges LD, Joseph DD (1980) A normal stress amplifier for the second normal stress difference. J Nonnewton Fluid Mech 6:325–331. https://doi.org/10.1016/0377-0257(80)80009-7

Sui C, McKenna GB (2007) Instability of entangled polymers in cone and plate rheometry. Rheol Acta 46:877–888. https://doi.org/10.1007/s00397-007-0169-8

Takahashi T, Fuller G (1996) Stress tensor measurement using birefringence in oblique transmission. Rheol Acta 35:297–302. https://doi.org/10.1678/rheology1973.24.3_111

Takahashi T, Shirakashi M, Miyamoto K, Fuller GG (2002) Development of a double-beam rheo-optical analyzer for full tensor measurement of optical anisotropy in complex fluid flow. Rheol Acta 41:448–455. https://doi.org/10.1007/s00397-002-0226-2

Tanner RI (2000) Engineering rheology, 2nd edn. Oxford University Press, New York

Tanner RI (1970) Some methods for estimating the normal stress functions in viscometric flows. Trans Soc Rheol 14:483–507. https://doi.org/10.1122/1.549175

Tanner RI (1973) A correlation of normal stress data for polyisobutylene solutions. Trans Soc Rheol 17:365–373. https://doi.org/10.1122/1.549317

Tanner RI, Keentok M (1983) Shear fracture in cone-plate rheometry. J Rheol 27:47–57

Tanner RI, Pipkin AC (1969) Intrinsic errors in pressure-hole measurements. Trans Soc Rheol 13:471–484. https://doi.org/10.1122/1.549147

Wang SQ, Ravindranath S, Boukany PE (2011) Homogeneous shear, wall slip, and shear banding of entangled polymeric liquids in simple-shear rheometry: a roadmap of nonlinear rheology. Macromolecules 44:183–190. https://doi.org/10.1021/ma101223q

Wineman AS, Pipkin AC (1966) Slow viscoelastic flow in tilted throughs. Acta Mech 2:104–115

Xu X, Chen J, An L (2014) Shear thinning behavior of linear polymer melts under shear flow via nonequilibrium molecular dynamics. J Chem Phys 140:174902. https://doi.org/10.1063/1.4873709